Alemi et al., *BioImpacts*, 2022, 12(x), x-x
doi: 10.34172/bi.2022.23820
http://bi.tbzmed.ac.ir/

Synthesis, characterization, and evaluation of pH-sensitive doxorubicin-loaded functionalized graphene oxide in osteosarcoma cells

Forough Alemi[1,2#], Masomeh Maleki[2#], Mostafa Mir[3], Abbas Ebrahimi-Kalan[4], Mojtaba Zarei[5,6], Bahman Yousefi[1,6*], Nadereh Rashtchizadeh[1,7*]

[1]Student Research Committee, Tabriz University of medical sciences, Tabriz, Iran
[2]Department of Biochemistry and Clinical Laboratories, Faculty of Medicine, Tabriz University of Medical Sciences, Tabriz, Iran
[3]Metabolic Disorders Research Center, Golestan University of Medical Sciences, Gorgan, Iran
[4]Department of Neurosciences and cognition, Faculty of Advanced Medical Sciences, Tabriz University of Medical Sciences, Tabriz, Iran
[5]Molecular Medicine Research Center, Tabriz University of Medical Sciences, Tabriz, Iran
[6]Drug Applied Research Center, Tabriz University of Medical Sciences, Tabriz, Iran
[7]Connective Tissue Diseases Research Center, Tabriz University of Medical Sciences, Tabriz, Iran

Article Info

Article Type:
Original Article

Article History:
Received: 5 May 2021
Revised: 6 Dec. 2021
Accepted: 18 Dec. 2021
ePublished: 13 Aug. 2022

Keywords:
Doxorubicin
GO nanosheet
Osteosarcoma
Quaternized imidazolium
Tris-modified GO

Abstract

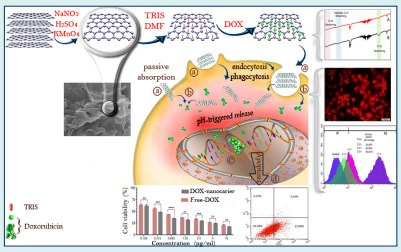

Introduction: Doxorubicin (DOX) is one of the most common drugs in cancer treatment. However, its partial solubility along with the high incidence of side effects remains a challenge to tackle. To address these issues, we designed a formulation based on graphene oxide (GO) and used it as an anticancer drug delivery system.

Methods: The physical and chemical properties of the formulation were studied using FTIR, SEM, EDX, Mapping, and XRD. Release studies in the *in vitro* condition were used to evaluate the pH sensitivity of drug release from nanocarriers. Other *in vitro* studies, including uptake assay, MTT, and apoptosis assay were carried out on the osteosarcoma (cell line.

Results: *In vitro* release studies confirmed that the synthesized formulation provides a better payload release profile in acidic conditions, which is usually the case in the tumor site. On the OS cell line, the cytotoxicity of the DOX-loaded nanocarrier (IC50=0.293 µg/mL) and early apoptosis rate (33.80%) were higher in comparison to free DOX (IC50=0.472 µg/mL, and early apoptosis rate= 8.31%) after 48 hours.

Conclusion: In summary, our results suggest a DOX-loaded graphene oxide carrier as a potential platform for targeting cancer cells.

Introduction

Osteosarcoma (OS) or primary bone cancer is the most common type of bone cancer in children and young adolescents, only after lymphoma and brain cancer.[1,2] Surgery, chemotherapy, or a combination of the two are common strategies for treatment.[3,4] Chemotherapeutic agents and their unfavorable side effects have been the subject of studies for decades and have not yet been addressed properly.[5,6] Doxorubicin (DOX) is a common chemotherapeutic agent that intercalates with double-strand DNAs of cancer cells and disrupts its replication process. However, at the same time, it negatively affects the normal cells in the heart, liver, kidney, and brain.[7,8] Multidrug resistance, poor solubility of drugs, and narrow therapeutic windows are other common problems of traditional cancer medications.[9,10] To solve these problems, various nanoparticle-based drug delivery systems have been developed, in which drugs loading into/onto the nanocarriers.[11-17] Numerous organic and inorganic nanoparticles have been developed for the delivery of biological agents.[18-23] Among these, carbon-based platforms, such as graphene, are quite interesting and have unique features such as extremely high surface area per unit volume, high potential for chemical treatments and surface modifications, and ease of preparation as well as high mechanical and chemical stability.[24]

#Forough Alemi and Masomeh Maleki have contributed equally.
*Corresponding authors: Bahman Yousefi, Email: yousefib@tbzmed.ac.ir; Nadereh Rashtchizadeh, Email: rashtchizadeh@rocketmail.com

Graphene oxide (GO) is a single atomic layer of carbon atoms, with epoxy, hydroxyl, and carboxyl functional groups on the surface which provides an exceptional opportunity for linking various biologically active components.[25,26] Mechanistically, GO nanosheets can be internalized through various routes by mammalian cells, spanning a diverse range from micropinocytosis to microtubules dependent pathways as well as phagocytosis and clathrin-mediated endocytosis.[27] However, in the MG63 OS cell line and other non-phagocytic mammalian cell lines, plasma membrane damage and the production of ROS are the main mechanisms of toxicity by GO and its derivatives. Concerning the outstanding physical, chemical, and optical properties of GO nanomaterial its potential biomedical applications have not been investigated thoroughly.

The solid tumors microenvironment has acidic pH due to the high rate of glycolysis and great lactic acid generation.[28] Targeted therapy could employ this feature of cancer cells to deliver therapeutic agents to the tumor microenvironment. In this study, in order to increase the concentration of DOX in the tumor microenvironment and decrease drug accumulation in healthy tissues, we have designed an acidic pH-sensitive GO-based drug carrier. In our nanocarrier, tris-modified GO was covalently linked to methyl imidazole molecules using ring-opening polymerization (ROP). Due to the large surface area of GO nanoparticles and numerous branches created on its surface by tris, this platform was used for high loading and delivering DOX to the OS cancer cell line. We utilized various characterization techniques such as Fourier-transform infrared spectroscopy (FTIR), energy-dispersive x-ray spectroscopy (EDS), energy dispersive x-ray analysis (EDX) mapping, scanning electron microscopy (SEM), and X-ray diffraction (XRD) analysis, in different steps of preparing our formulation for confirming its physical and chemical properties. Subsequently, loading and release profiles were calculated, and the efficacy of formulation was tested using biological assays, including quantitative and qualitative uptake assays, Thiazolyl blue tetrazolium bromide (MTT) assay, and apoptosis assay on the MG63 cell line. The importance of this work is that it uses relatively simple and easy steps as well as cheap materials to oxidize, functionalize and activate the biologically inert GO, which has a unique surface area to volume ratio, for the delivery of an active anticancer substance to the tumor site.

Materials and Methods

Materials

Epichlorohydrin (ECH, 99%), 1-methylimidazole (MI, 99%), dimethylsulfoxide (DMSO), and 4′,6-diamidino-2-phenylindole (DAPI) were provided from Sigma-Aldrich, St. Louis, MO, USA. Solvents and chemical reagents were purchased from Merck, Branchburg, NJ, USA. Roswell Park Memorial Institute (RPMI) 1640 growth medium, fetal bovine serum (FBS), and trypsin were purchased from Gibco BRL Life Technologies, Grand Island, NE, USA. DOX powder was provided from Sobhan Pharmaceutical Company, Tehran, Iran. MTT was obtained from Bio Basic Inc., Markham, Canada. Quaternized imidazolium (QI) and quaternized imidazolium-functionalized oxirane (QIFO) were synthesized according to the recent literature.[29,30]

Instrumentation

FTIR spectroscopy was used for the characterization of all chemical structures and recorded on a Bruker Tensor 270 spectrometer (Burker, Massachusetts, NE, USA). To measure the zeta-potential and average diameter of nanosheets, the laser-scattering technique was performed at 25°C by Zetasizer Nano ZS90; Malvern Instruments, Malvern, United Kingdom. All samples were spread on an SEM stub and sprinkled with gold and studied with a field emission SEM (FESEM) and EDX to determine the size, surface morphology, and elemental study of nanosheets (FESEM instrument of ZEISS company, Sigma VP; Oberkochen, Germany). To characterize the structure of the crystal phase, XRD measurements using Cu Kα radiation were done X' Pert Pro, Malvern Panalytical Ltd, Malvern, United Kingdom.

Preparation of Drug Carrier

Preparation of pure GO

0.6 g of graphite, 25 mL of H_2SO_4, and 0.6 g of $NaNO_3$, were stirred in an ice bath for 1 h. Afterward, $KMnO_4$ (1.6 g) was solved by stirring at 35 ℃ for 24 hours to reach a thick solution. Then, 25 mL of de-ionized water was gently added to this mixture to control the reaction temperature (up to 90℃) and stirred for 30 min. At that time, 7 mL of H_2O_2 (30 %) and 75 mL of de-ionized water were added. This mixture was then filtered using a gravity filter and washed alternately with deionized water and 5% HCl solution several times. Finally, the product was freeze-dried to avoid GO aggregation.[31]

Preparation of Tris-GO (TRIS-GO)

For surface functionalization of GO, 3.0 g of TRIS was dissolved in 100 mL dried DMF, and then 1.0 g of GO was added to the solution and stirred for two days at room temperature. Subsequently, the sediment was separated with a 15-min centrifugation step at 5000 x g. Deionized water was used to wash this solution, and then it was dried at room temperature.[32]

Preparation of functionalized GO (FGO)

For activating the hydroxyl groups on the GO surface 0.25 g of GO-TRIS was dissolved in 25 mL of deionized water and its pH was brought to 11 by the addition of NaOH (2 M). An ultrasonic bath was used to disperse for 1 hour followed by using a magnetic stirrer at 50°C for 24 hours. The obtained suspension was added drop by drop to the QIFO solution and stirred again for 24 hours. The resulting mixture was centrifuged at 6000 x g for 15

minutes to remove the excess reagents and then washed twice and dried in the vacuum.

DOX loading

To load DOX on the drug carrier, 50 mg of FGO was dispersed in 0.5 mg/mL DOX solution and stirred for 24 hours in a dark condition at room temperature. After centrifugation for 5 minutes at 2000 x g, the supernatant absorbance was measured by UV-VIS spectrophotometry at 480 nm. To calculate the concentration of unloaded DOX calibration curve from different concentrations of free DOX was drawn. Drug encapsulation efficiency and drug loading efficiency of DOX were calculated by the following formulas.

$$\text{Drug Loading efficiency } (\% \frac{w}{w}) = \frac{\text{mg of DOX in the FGO}}{\text{mg of the FGO}} \times 100$$

$$\text{Drug encapsulation efficiency } \left(\% \frac{w}{w}\right) = \frac{\text{mg of DOX in the FGO}}{\text{mg of feeded DOX}} \times 100$$

The obtained precipitate was washed with PBS and vacuum dried for further *in vitro* studies such as MTT assay and cell uptake assay.

DOX release

To evaluate the release rate of DOX from nanocarrier, 4 mg of DOX-FGO was dispersed in 10 ml of phosphate-buffered saline (PBS) solution in various pH solutions (7.4, and 5.2). All of these solutions were shaken in a 37°C incubator for pre-determined interval times. The supernatant absorbance was measured by the UV-vis spectrophotometer at a wavelength of 480 nm. The DOX concentration was calculated using the calibration curve.

Cell culture and MTT assay

For the measurement of cytotoxicity, an MTT assay was used.[33] The MG-63 cells were cultured in RPMI medium (containing streptomycin and penicillin) with 10% FBS and incubated at 37°C (with 95% humidity and 5% CO_2). To assay cytotoxicity, 10 000 cells were seeded per well in the 96 well plates, and 200 µL of culture medium was added with 10% FBS to each well.[34] The plates were incubated at 5% CO_2 and in a humidified atmosphere for 24 hours at 37°C so that the cells have enough time to stick to the bottom of the wells. After preparing serial dilutions, the cells were treated with indicated concentrations of FGO, free DOX, and DOX-FGO (10, 5, 2.5, 1.25, 0.625, 0.312 µg/ mL). The concentrations of DOX-FGO were based on the content of DOX. A control group without treatment for each of these groups was considered. Each of the wells was washed two times with PBS after 48 hours of incubation. Then, a 180 µL growth medium with 10% FBS and 20 µL MTT solution was added to each well and incubated for 4 hours. After this period, the contents were removed and 150 µL DMSO was added to each well to solve the crystals of formazan. ELISA reader (Awareness Technology, Palm City, FL, USA) at 570 nm was used to determine the absorbance of the formazan. All tests were performed in triplicate. The following formula was used to calculate the cell viability:

$$\text{Cell viability } (\%) = \frac{\text{The absorbance of each test}}{\text{Mean absorbance of controls}} \times 100$$

Cellular uptake assay

Fluorescence microscopy and flow cytometry were implemented to evaluate the qualitative and quantitative cellular uptake of the DOX-FGO. For this purpose, 5×10^5 MG-63 cells per well were seeded in six-well plates and 24 hours incubated. Then these cells were treated with DOX-FGO at IC_{50} value (0.293 µg/mL) for 0.5, 1, and 2 hours. Finally, the cells were eluted with PBS and the cellular uptake was assessed and analyzed by FACSCalibur flow cytometry. (Becton Dickinson Immunocytometry Systems, San Jose, CA, USA). The quantitative intracellular uptake test with flow cytometry was repeated for free DOX.

To evaluate cellular uptake by fluorescence microscopy, MG-63 cells were seeded in a slide chamber (4×10^4 per chamber) and incubated for 24 hours. Cells were treated with DOX-FGO at the IC_{50} value for 0.5, 1, and 2 hours, then chambers were washed with PBS and red fluorescence of DOX was detected with fluorescence microscopy (Olympus microscope Bh2-RFCA, Tokyo, Japan).

Apoptosis assay

To evaluate if cell death is apoptosis 500×10^3 MG-63 cells per well were seeded into six-well plates in the RPMI and for 24 hours incubated at 37°C. The RPMI medium was replaced with a new medium, and then cells were treated with IC_{50} values of free DOX, DOX-FGO, and blank FGO. After 48 hours of incubation, the cells were trypsinized and centrifuged to remove all trypsin. Then, the cells were collected and washed with PBS.[35] Subsequently, 1 mL annexin binding buffer for 1×10^6 cells was used to stain the apoptotic cells. A eBioscience™ Annexin V-FITC Apoptosis Detection Kit (eBioscience, Inc., San Diego, CA, USA) was used for apoptosis assay, according to the manufacture's protocol. In brief, 100 µL of cell suspension were mixed with 5 µL FITC Annexin V, and 5 µL propidium iodide (PI). After 15 minutes incubation, 400 µl buffer was added to each suspension. Finally, results were analyzed with a FACSCalibur flow cytometer.

Statistical analyses

Statistical analysis was performed via GraphPad Prism 6 software (GraphPad Software, Inc., La Jolla, CA). Kolmogorov-Smirnov's normality test was applied for evaluating the normal distribution of data. Independent two samples *t* test was performed to determine the significant differences between free DOX and their nanoformulations results at different concentrations in 24 and 48 hours. In addition, significant differences are shown as * $P < 0.05$, ** $P < 0.01$, *** $P < 0.001$ and **** $P < 0.0001$.

Results

Preparation and characterization

Surface modification of GO with QI was performed for DOX loading (Fig. 1) as an anticancer drug and used for the treatment of MG-63 cells. The following characterizations were used for analyzing the samples in each step and discussed as well.

As seen in Fig. 2A, the FTIR spectrum of Tris-GO has three characteristic peaks. A peak at around 1043 cm^{-1} is attributed to C-O stretching bonds. The C=O bond in carboxylic acid at the edge of the GO sheets is observed at around 1718 cm^{-1}. The peak at around 2879-2948 cm^{-1} is related to the C-H aliphatic stretching bonds. The O-H stretching band is also observed at 3419 cm^{-1}. After modification by the ROP approach with QIFO, the FTIR spectrum did not show significant changes, however, the intensity of the peaks at around 1053 cm^{-1} is increased due to the increasing number of C-O bonds in the polymeric network of QI-functionalized branches. Interestingly, the intensity at around 2858-2923 cm^{-1} is slightly enhanced due to a similar reason. Observed peaks at around 1500 cm-1 are mainly due to c=c stretching which is the building block in graphene.

The samples were also analyzed with the XRD technique to show the changes in the crystallinity of the Tris-GO and FGO. As shown in Fig. 2B, the XRD graphs of both samples have a different pattern. Tris-GO has no changes in morphology and structure after modification, thus, it has a crystalline structure with a very sharp peak at 10.52° and a slightly intense peak of 43.37°. After surface modification, the peak at 10.52° disappears and the peak at 43.37° is enhanced. Also, a broad peak at 19.17° is observed.

SEM images were obtained to study the morphology and structure of the nanosheets before and after treatment. As can be seen in Fig. 2C, untreated GO (as our control) has a morphology of crumpled paper; a rather planar surface with a number of ripples, wrinkles, and folds on it, each folded plane has an average thickness of 55 nm. Fig. 2C shows, as expected in the morphologic structure of Tris-GO nanosheets, that no significant changes have occurred. However, after the polymerization reaction on Tris-GO nanosheets, there are some morphological changes in the surface of nanosheets, including an increase in plate wrinkles and also an increase in the surface roughness. Homogeneous corrugated surface of sheet-like structures was observed in all samples which is in accordance with previous studies.[36]

EDX mapping analysis was performed for the determination of element percentage in a semi-quantitative approach and their distribution on the surface of the modified platforms. Fig. 3 depicts the EDX analysis of GO, Tris-GO, and FGO showing logical results. GO has only two detectable elements (carbon and oxygen) by EDS analysis and is about 65% w and 35% w for carbon and oxygen, respectively. After grafting Tris on the surface of GO, it is expected that the nitrogen element also can be detected by EDS analysis. The results show that the weight percentage of carbon, oxygen, and nitrogen is 59.37%, 16.94%, and 23.69%, respectively. (Fig. 1D) The polymeric network of the platform after modification with QI moiety has no new elements other than carbon, nitrogen, and oxygen; therefore, as expected just some changes in the weight percentages are observed. Fig. 3

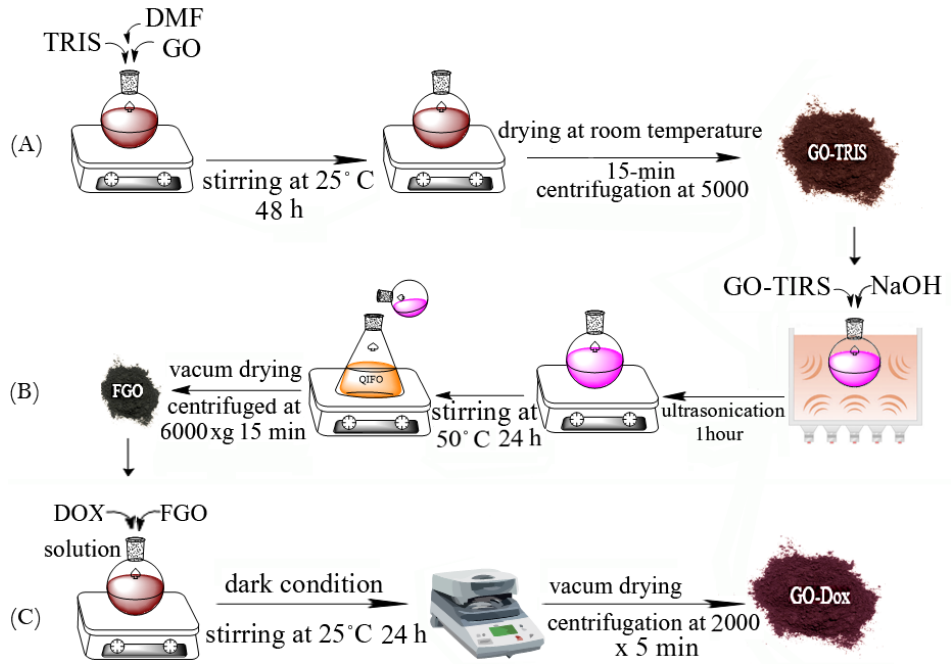

Fig. 1. Preparation process of doxorubicin (Dox) loaded functionalized graphene oxide (GO) (A) preparation of TRIS functionalized GO. (B) preparation of activated GO. (C) preparation of Dox-loaded GO nanoparticles.

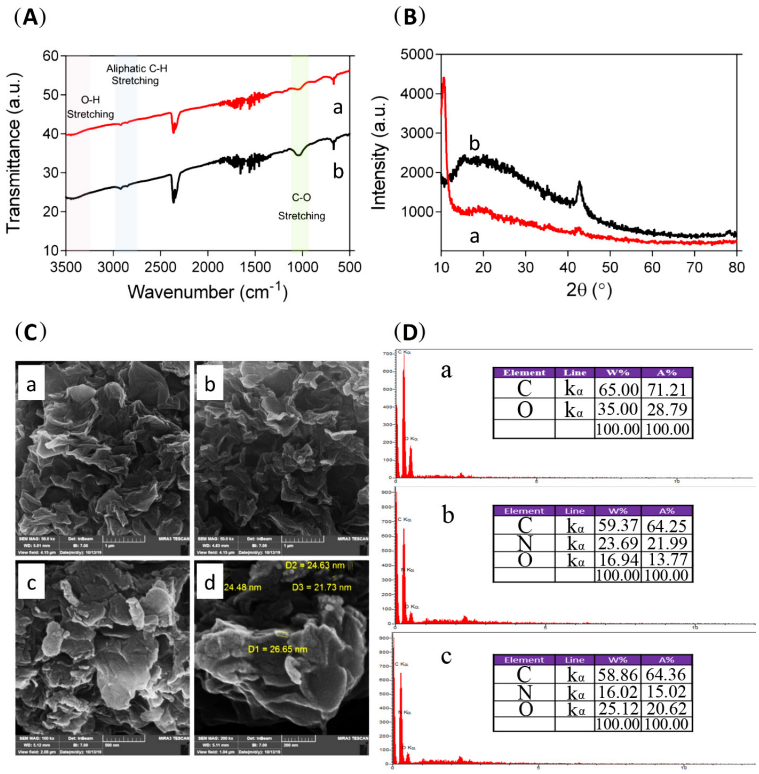

Fig. 2. The characterization of graphene oxide (GO) and its functionalized derivatives (A) FTIR spectra of Tris- graphene oxide (GO) (a) and functionalized graphene oxide (FGO) (b). (B) XRD graphs of Tris-GO (a), and FGO (b). (C) SEM images of GO (a), GO-Tris (b), and FGO (c and d). (D) EDS analysis of GO (a), Tris-GO (b), and FGO (c).

shows the distribution of the elements in each sample. This technique confirmed that surface modification was done successfully and uniformly.

In vitro DOX loading and release study

After 24 hours of incubation in dark conditions and several washing processes, the supernatant was collected and its optical density was measured at 480 nm. Using the DOX calibration curve, loading efficiency, and encapsulation efficiency were measured as 9.91% and 99.1%, respectively. For testing the sensitivity of the nanoformulation to pH variation, we performed the *in vitro* release study. Results over 25 days show that DOX release from nanocarrier at pH=5.2 and pH=7.4 at body temperature was 53% and 37%, respectively (Fig. 4). For a better and more detailed understanding of release kinetic and possible involved mechanisms (whether its diffusion, dissolution, or erosion) the release curves were fitted to various models including; zero-order (Fig. 5A,B), Korsmeyer–Peppas model (Fig. 5C), and Higuchi's model

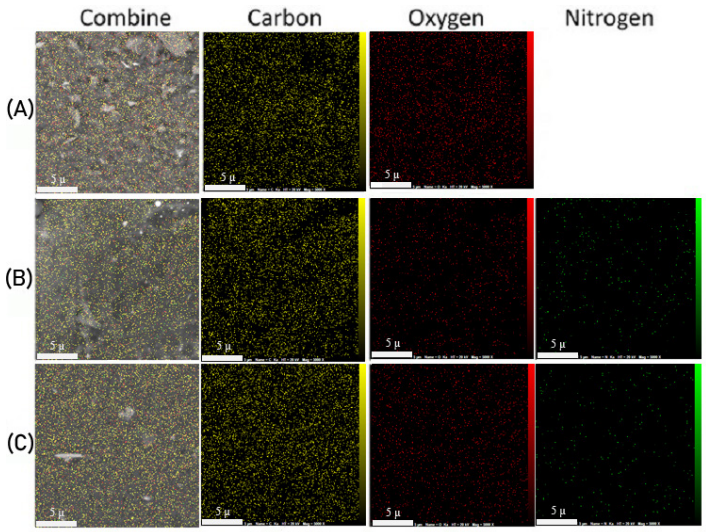

Fig. 3. EDX mapping analysis of (A) graphene oxide (GO), (B) Tris-GO, and (C) functionalized GO (FGO).

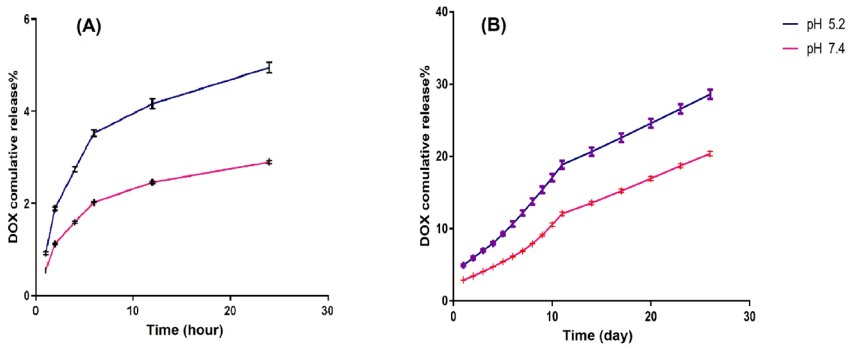

Fig. 4. The cumulative release of doxorubicin (Dox) at various pH values (5.2, and 7.4) at 37°C (A) in the first 24 hours (B) in 25 days.

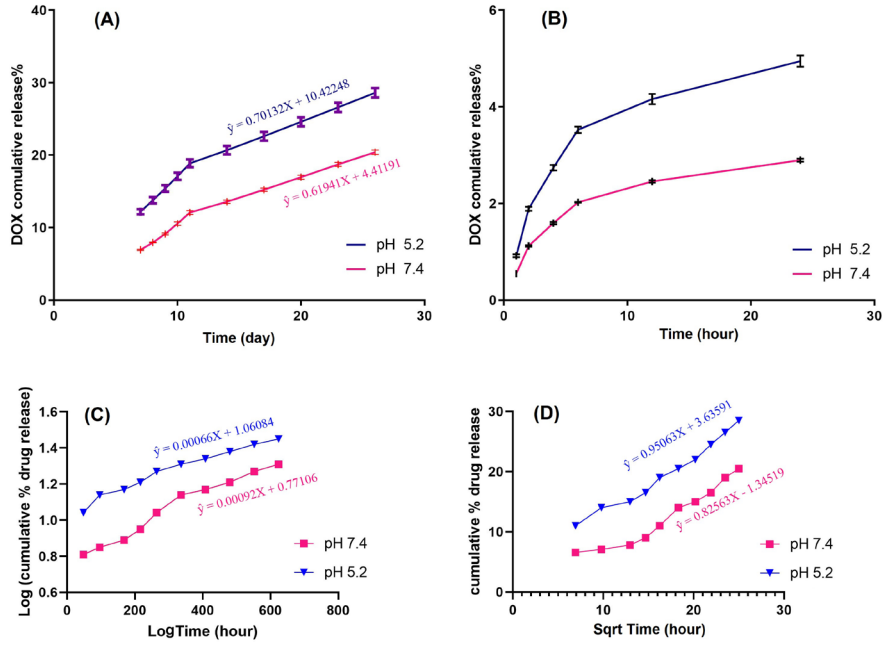

Fig. 5. Drug release plot fitted to various kinetic models. (A) and (B) Zero order (C) Korsmeyer-Peppas model (D) Higuchi model.

(Fig. 5D) and first-order model based on the following equations:

Higuchi's model: $Q_t/Q_0 = 2(D_t/\pi) = K_H\, t^{1/2}$

Korsmeyer–Peppas model: $Q_t/Q_0 = K_n\, t$

Zero order: $Q_t/Q_0 = K_0\, t$

First order: $\ln Q_t/Q_0 = K_1\, t$

Q_0 and Q_t correspond to the original drug concentration and concentration of drug released at time t. D and K are diffusion and release coefficients respectively. Table 1 represents the calculated values of correlation coefficient (r^2) and equation constants based on various kinetic models.[37,38]

For our formulated GO-Dox nanocarrier calculated values of correlation coefficient (r^2 = 0.9918) suggest Korsmeyer–Peppas (Fig. 5C) diffusion as the preferred and dominant mechanism of release in both pH values. In addition, the calculated value of release exponent from Korsmeyer–Peppas equation (n) in both pH is more than

Table 1. Drug release kinetics, correlation coefficient values, and equation constants of different kinetic models

	Correlation coefficient (r^2)				n (Korsmeyer-Peppas constant)	K (Korsmeyer-Peppas constant)	K_H (Higuchi's constant)
GO-Dox	Zero order	First order	Korsmeyer–Peppas	Higuchi			
pH= 5.2	0.9646	0.9785	0.9918	0.925	0.515	1.18	$1.1*10^{-3}$
pH= 7.4	0.9731	0.9805	0.983	0.869	0.633	0.36	$0.75*10^{-3}$

0.45 which is indicative of non-Fickian (anomalous) diffusion of drug from nanoparticle surface.

Intracellular uptake

For measuring the amount of internalized nanoformulation, quantitative and qualitative uptake tests were performed on MG63 cells. The fluorescence microscopy images (Fig. 6A) showed that a significant amount of formulation was internalized by MG63 cells. As can be seen, the internalization process was completed in the first few hours of exposure to the nanoformulation. Flow cytometry as the quantitative evaluation was performed for free DOX and DOX-nanocarrier. It can be seen that 99.48% of DOX- nanocarrier were internalized by MG63 cells after 2 hours (Fig. 6B). The rate of the free-DOX uptake was 99.90% after 1 hour (Fig. 6C).

MTT cytotoxicity assay

MTT assay was performed to compare and evaluate the efficacy of free DOX, nanocarrier, and DOX-nanocarrier in cell growth at 24 and 48 hours timescales (Fig. 7). GO nanosheets did not show a toxic effect on the growth of the MG-63 cells even at high concentrations (10 µg/mL). For evaluating and comparing cytotoxicity of formulation and free drug, cells were treated with different concentrations of the drug and formulations. After 24 and 48 hours values of IC_{50} were measured for DOX-nanocarrier as 3.733 µg/mL and 0.293 µg/mL respectively. The IC_{50}s of free DOX after 24 and 48 hours were 7.347 µg/mL and 0.472 µg/mL, respectively.

Apoptosis assay by flow cytometry

Derivatives of GO alongside several GO-based formulations have been shown to be capable of inducing apoptotic pathways in human cancer cells.[39] After treatment with DOX-nanocarrier, free DOX, and bare nanocarrier for 48 h, samples were used to evaluate apoptosis using annexin V/PI and flow cytometry (Fig.8). Untreated cells were used as the control group (Fig. 8A). As depicted in Fig. 8, similar to the MTT assay the flow cytometry analysis showed that the treatment of the bare nanocarrier for MG-63 OS cell lines is safe in a drug delivery system (Fig. 8B). On the other hand, cells treated with free DOX (Fig. 8C) and DOX-nanocarrier (Fig. 8D) were positive for annexin V/PI. Indeed, the treatment of MG-63 OS cell lines with free DOX and DOX-nanocarrier for 48 hours resulted in 8.31% and 33.80% early apoptotic cells as well as 6.52% and 0.45% late apoptotic cells, respectively.

Discussion

Investigation of potential carriers for the delivery of chemotherapeutic agents is crucial for the development of next-generation cancer treatments. Here we designed a

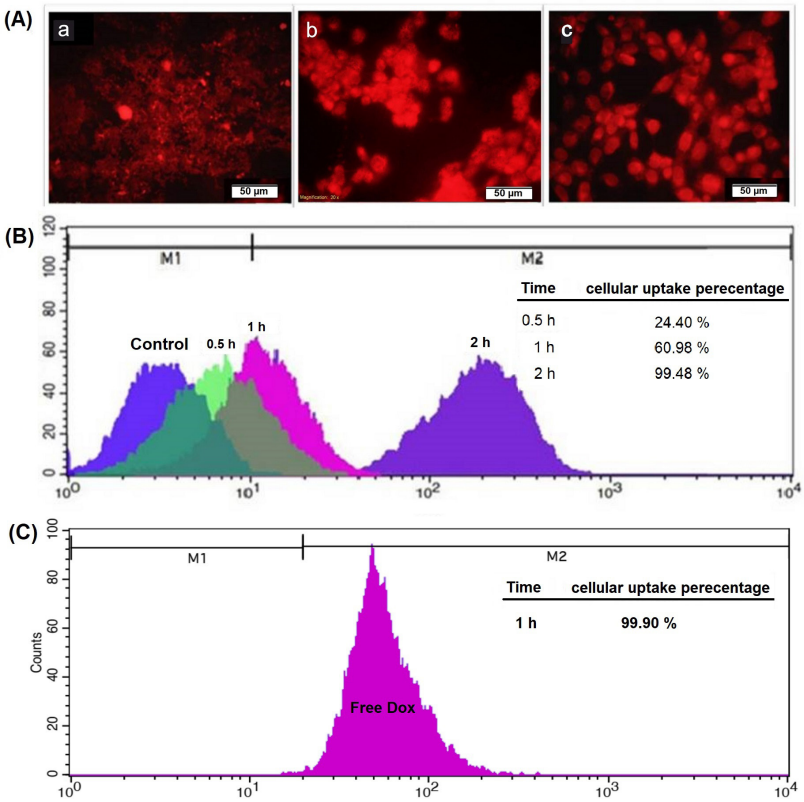

Fig. 6. Cellular internalization of the DOX/nanocarrier. (A) Fluorescence microscopy images of DOX-nanocarrier uptake by MG-63 cells for 0.5 (a), 1(b), and 2 (c) hours. (B) Cellular uptake percentage of DOX-nanocarrier by MG-63 cells for 0.5, 1.0, and 2.0 hours after treatment. (C) Cellular uptake percentage of free-DOX after 1.0-hour treatment.

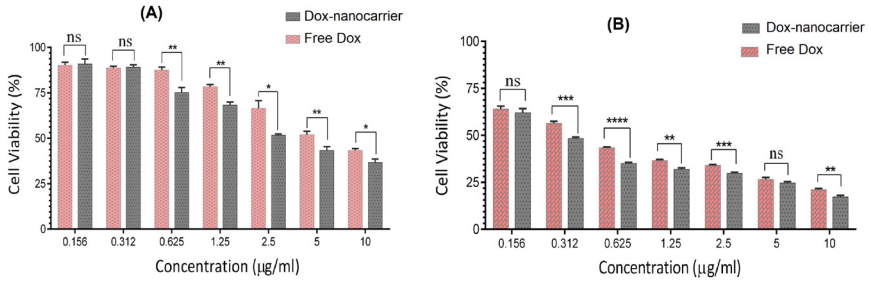

Fig. 7. Cell growth inhibition rate by different concentrations of free DOX, and DOX-nanocarrier after (A) 24 and (B) 48 hours of treatment. ns; none significant, **P* < 0.05, ***P* < 0.01, ****P* < 0.001.

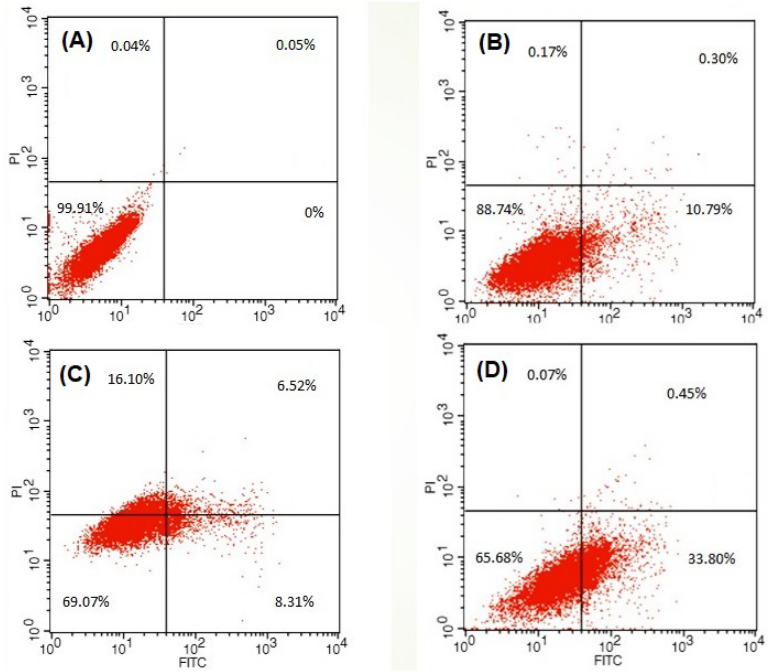

Fig. 8: Evaluation of the apoptosis with flow cytometry after 48 hours treatment of MG-63 cells with (A) treated with full media for control, (B) nanocarrier (10 µg/ml), (C) free DOX (0.472 µg/mL), (D) DOX-nanocarrier (0.293 µg/mL). after (A) 24 and (B) 48 hours of treatment. ns; none significant, **P* < 0.05, ***P* < 0.01, ****P* < 0.001.

study to show that tris-FGO could be a potential platform for the delivery of DOX as a standard chemotherapeutic agent.

The presence and intensity of hydroxyl, carbonyl and carboxyl functional groups confirmed that the graphite is optimally oxidized into GO and according to the literature the degree of oxidation is acceptable to be used in the next step.[40] The abundance of C=C groups (which is the backbone and building block of GO structure) in all samples showed that, during the oxidation of graphite into GO, the main structure is preserved. We normally do not expect to observe a distinct peak after imidazolium-functionalization because the subsequent peaks of N-H and C-N overlap with that of O-H and C=O respectively.[41] The obtained FT-IR results confirmed that GO was successfully synthesized, and functionalized to be loaded with DOX.

GO has two distinctive and characteristic (001) sharp XRD peaks at 2θ=10.52° and a small (100) at 2θ=43.37°. The d-spacing is calculated to be d= 0.845nm. This large d-spacing is attributed to the formation of hydroxyl, epoxy, and carbonyl functional groups during the oxidation of graphite, so the presence of 2θ=10.52° is an indicator of successful GO oxidation from graphite and the shift of XRD peak of graphite at 2θ = 26.5° to 10.52° in GO has been interpreted in the literature as the indicator of successful oxidation of graphite sheets.[42] After imidazolium functionalization the sharp XRD peak at 2θ=10.52° changed to a broad peak at 2θ=19.17° and subsequently, d-spacing is reduced to d= 0.445nm which indicated that the oxygen-containing functional groups have been reduced during imidazolium functionalization.[43]

Morphological analysis using SEM showed that the images are empty of any big chunks of unoxidized graphite and it has the typical creased texture of a wrinkled paper containing lots of ripples and folding on it, which indicates an acceptable degree of oxidation and exfoliation.[44] Functionalization of GO sheets normally does not alter the structure or morphology of sheets but upon close inspection, it can be seen that the texture has been shifted from a wrinkled paper to a crushed stone, which can be interpreted as the result of proper oxidation and reduction processes during the synthesis and drug loading.[45]

Observing elemental distribution on samples using EDX confirmed the success of each step and is in accordance with other characterization data. The presence and well-dispersed oxygen atoms on the surface of the nanoparticles confirmed that Graphene sheets have been oxidized optimally C/O ratio of roughly 1.85 shows us an acceptable ratio of oxidation for GO. Most literature introduces an average of 1.5 to 3 as the optimal degree of oxidation.[46] well-dispersed nitrogen atoms from tris functionalization appeared in the EDX map in Figs. 3B and 3C and confirm the introduction of nitrogen atoms (by 23 present mass) into the composition of GO via tris modification. A roughly ten percent increases in the ratio of oxygen represent the functionalization by QI molecules to the nanocarrier composition.[47] Which is evident in a close comparison of oxygen maps of sections B and C in Fig. 3.

Previous studies showed that the drug loading ratio of GO could reach 200%[48] (almost twice as much as other nanoparticles) due to its vast surface area. GO's surface area is about 2600 m^2/g, which is higher than most other nanomaterials.[49] FGO, in the same way, offers a great surface area to volume ratio, and because of the presence of carboxyl, and hydroxyl functional groups on its surface, which are sites for electrostatic bonding, we expected an excellent drug loading capability. Also, due to the high solubility and disparity of DOX and FGO in PBS and their opposite ionic charges, we could easily link DOX to nanocarrier with covalent bond connections (1:10). High encapsulation efficiency (99.1%) for DOX proves that FGO is a carrier with exceptional loading capacity. However, as the H^+ concentration increases in acidic media, these covalent bonds are destroyed, and the release of the DOX from the nanocarrier increases. A study by Vinothini et al showed that DOX was slowly released at pH-5.5 (endosomal pH of cancer cells) and pH-6.8 (neutral pH) from a GO nanoformulation, but a high amount of drug release rate was observed under acetic condition pH-2.8.[50] According to our results of the release test (Fig. 4), we conclude that drug release in acidic pH (5.2) was higher in comparison to physiological pH (7.4), which consequently can improve that DOX-FGO is a pH-sensitive nanoparticle. pH sensitivity is a reason for high concentrations of DOX in the tumor microenvironment and within tumor cells that have uptaken the nanoparticles. In addition, fitting the release curves based on common release kinetic models and calculating the correlation coefficient showed that the release mechanism is closest to the Korsmeyer–Peppas diffusion model (also known as Power law). This system describes drug release from polymeric systems, porous materials, and nanoparticles in which there are several structural and nano-geometrical interactions between a drug and its carrier. It can be inferred that tris modifications act as small nano-sized mesh on the surface of GO nanoparticles and gives them a polymeric behavior.[51,52]

MTT assay showed the high viability of MG-36 cells treated with FGO even in high concentrations, which made it a safe and biocompatible carrier for the delivery of drugs and biological agents. From the obtained data it can be concluded that after 24 hours cytotoxic effects of DOX-FGO on MG-63 were not significantly different from the free DOX but after treatment for 48 h, the cytotoxic effect of DOX-FGO improved, and its IC_{50} decreased. Accordingly, results indicated that cytotoxicity of free DOX and DOX-FGO had a time-dependent characteristic, and IC_{50} decreased over time. The high loading capacity of FGO could be a reason for the high concentration of DOX inside the cells which uptake nanoformulation and cause lower viability of these cells. This has been confirmed with the uptake test. The internalization rate showed that a significant amount of nanoformulation was internalized by MG63 cells and appeared in florescent microscopy photographs and flow cytometry uptake results. As can be seen, the internalization process was time-dependent and almost completed after 2 hours of exposure to the nanoformulation (Fig. 6B). In general, based on the size of GO nanosheets, mechanisms of internalization may vary from clathrin-mediated endocytosis for smaller nanosheets to phagocytic uptake for larger ones. Additionally, there is some evidence for passive uptake of GO nanosheets.[53] These findings could explain why internalization of DOX-FGO takes more time (60.98% after 1h presented in Fig. 6B). However, free DOX enters the cytoplasm by diffusion and quickly binds to the proteasome's 20S subunit. This complex can diffuse into the nucleus[54] and is observed in the cytoplasm and nucleus of cells in 1 h, which is confirmed by the result of free DOX uptake (99.90% after 1h presented in Fig. 6C). There are pieces of evidence that show that prolonged exposure of cells with DOX, in addition to nuclear apoptosis, could also activate the mitochondrial apoptotic pathway.[55,56] The accumulation of ROS inside the cells is one of the cellular events caused by DOX, which ultimately leads to p53 phosphorylation and apoptosis.[57] This evidence could explain the lower IC50 of nanoformulation in campier with free DOX in a long exposer time (48 hours). The apoptosis results are also in line with MTT findings. The degree of early apoptosis in DOX-FGO treated cells was 33.80%, higher than the early apoptotic rate of cells treated with free DOX (8.31%) after 48 hours, which confirms the cells going to apoptosis

Research Highlights

What is the current knowledge?

√ DOX is a common chemotherapy agent for the treatment of OS.

√ The weaknesses of DOX are poor solubility and high side effects.

√ Nanoparticle-based drug delivery systems can help to overcome these weaknesses

What is new here?

√ DOX-loaded GO carrier can be considered a potential platform for targeting OS cells.

if the FGO-DOX exposure time increases. Based on the above-mentioned points we suggest the FGO nanocarrier as an ideal delivery system for DOX.

Conclusion

In this study, we designed a drug delivery system based on GO nanosheets to obtain a controlled release of DOX in MG63 cancer cells, as well as to reduce its side effects. GO nanosheets were functionalized and DOX was linked onto its surface using electrostatic interactions. Outstanding surface area to volume ratio and consequently exceptional capacity for drug loading, and responsiveness to pH are some of the features of our nanoformulation. We used MTT assay, cellular uptake assay, apoptosis assay, and flow cytometry to confirm the efficacy of DOX-FGO as a delivery system. Our study recommends that the present modified GO could sensitize OS cells to DOX, indicating the desirability of performing *in vivo* studies in the future.

Acknowledgment

The authors would like to thank the Clinical Research Development, Unit, Shohada Hospital, and Tabriz University of Medical Sciences for their kind support.

Funding sources

The research grant was provided by Clinical Research Development Unit, Shohada Hospital, Tabriz University of Medical Sciences (grant no: 64138).

Ethical statement

This study was approved by the ethical committee of Tabriz University of Medical Sciences (IR.TBZMED.REC.1398.1220)

Competing interests

The authors declare that they have no conflict of interest.

Authors' contribution

FA and MaM performed the experiments. MoM and MZ provided technical help. AEK was involved in data analysis. BY, and NR participated in the study design, manuscript drafting, and revising.

References

1. Haynes L, Kaste SC, Ness KK, Wu J, Ortega-Laureano L, Bishop M, *et al.* Pathologic fracture in childhood and adolescent osteosarcoma: A single-institution experience. *Pediatr Blood Cancer* **2017**; 64: e26290. https://doi.org/10.1002/pbc.26290
2. Botter SM, Neri D, Fuchs B. Recent advances in osteosarcoma. *Curr Opin Pharmacol* **2014**; 16: 15-23. https://doi.org/10.1016/j.coph.2014.02.002.
3. Alexandrino EM, Ritz S, Marsico F, Baier G, Mailänder V, Landfester K, *et al.* Paclitaxel-loaded polyphosphate nanoparticles: a potential strategy for bone cancer treatment. *J Mater Chem B* **2014**; 2: 1298-306. https://doi.org/10.1039/c3tb21295e
4. Shafabakhsh R, Reiter RJ, Mirzaei H, Teymoordash SN, Asemi Z. Melatonin: a new inhibitor agent for cervical cancer treatment. *J Cell Physiol* **2019**; 234: 21670-82. https://doi.org/10.1002/jcp.28865
5. Honari M, Shafabakhsh R, Reiter RJ, Mirzaei H, Asemi Z. Resveratrol is a promising agent for colorectal cancer prevention and treatment: focus on molecular mechanisms. *Cancer Cell Int* **2019**; 19: 1-8. https://doi.org/10.1186/s12935-019-0906-y
6. Shafabakhsh R, Asemi Z. Quercetin: a natural compound for ovarian cancer treatment. *J Ovarian Res* **2019**; 12: 1-9. https://doi.org/10.1186/s13048-019-0530-4
7. Armstrong J, Dass CR. Doxorubicin action on mitochondria: relevance to osteosarcoma therapy? *Curr Drug Targets* **2018**; 19: 432-8. https://doi.org/10.2174/1389450116666150416115852
8. Pourhanifeh MH, Sharifi M, Reiter RJ, Davoodabadi A, Asemi Z. Melatonin and non-small cell lung cancer: new insights into signaling pathways. *Cancer Cell Int* **2019**; 19: 1-7. https://doi.org/10.1186/s12935-019-0853-7
9. Majidinia M, Mirza-Aghazadeh-Attari M, Rahimi M, Mihanfar A, Karimian A, Safa A, *et al.* Overcoming multidrug resistance in cancer: Recent progress in nanotechnology and new horizons. *IUBMB Life* **2020**; 72: 855-71. https://doi.org/10.1002/iub.2215
10. Shafiei-Irannejad V, Samadi N, Salehi R, Yousefi B, Rahimi M, Akbarzadeh A, *et al.* Reversion of Multidrug Resistance by Co-Encapsulation of Doxorubicin and Metformin in Poly(lactide-co-glycolide)-d-α-tocopheryl Polyethylene Glycol 1000 Succinate Nanoparticles. *Pharm Res* **2018**; 35: 119. https://doi.org/10.1007/s11095-018-2404-7
11. Wu C, Fan W, Chang J. Functional mesoporous bioactive glass nanospheres: synthesis, high loading efficiency, controllable delivery of doxorubicin and inhibitory effect on bone cancer cells. *J Mater Chem B* **2013**; 1: 2710-8. https://doi.org/10.1039/c3tb20275e
12. Martínez-Carmona M, Lozano D, Colilla M, Vallet-Regí M. Lectin-conjugated pH-responsive mesoporous silica nanoparticles for targeted bone cancer treatment. *Acta Biomater* **2018**; 65: 393-404. https://doi.org/10.1016/j.actbio.2017.11.007
13. Kamba SA, Ismail M, Hussein-Al-Ali SH, Ibrahim TAT, Zakaria ZAB. In vitro delivery and controlled release of doxorubicin for targeting osteosarcoma bone cancer. *Molecules* **2013**; 18: 10580-98. https://doi.org/10.3390/molecules180910580
14. Lima AC, Ferreira H, Reis RL, Neves NM. Biodegradable polymers: an update on drug delivery in bone and cartilage diseases. *Expert Opin Drug Deliv* **2019**; 16: 795-813. https://doi.org/10.1080/17425247.2019.1635117
15. Prabakaran S, Jeyaraj M, Nagaraj A, Sadasivuni KK, Rajan M. Polymethyl methacrylate–ovalbumin@ graphene oxide drug carrier system for high anti-proliferative cancer drug delivery. *Appl Nanosci* **2019**; 9: 1487-500. https://doi.org/10.1007/s13204-019-00950-5
16. Rakhshaei R, Namazi H, Hamishehkar H, Rahimi M. Graphene quantum dot cross-linked carboxymethyl cellulose nanocomposite hydrogel for pH-sensitive oral anticancer drug delivery with potential bioimaging properties. *Int J Biol Macromol* **2020**; 150: 1121-9. https://doi.org/10.1016/j.ijbiomac.2019.10.118
17. Bahojb Noruzi E, Molaparast M, Zarei M, Shaabani B, Kariminezhad Z, Ebadi B, *et al.* Para-sulfonatocalix[n]arene-based biomaterials: Recent progress in pharmaceutical and biological applications. *Eur J Med Chem* **2020**; 190: 112121. https://doi.org/10.1016/j.ejmech.2020.112121
18. Rahimi M, Karimian R, Bahojb Noruzi E, Ganbarov K, Zarei M, S. Kamounah F, *et al.* Needle-shaped amphoteric calix[4]arene as a magnetic nanocarrier for simultaneous delivery of anticancer drugs to the breast cancer cells. *Int J Nanomedicine* **2019**; 14: 1-18.

https://doi.org/10.2147/IJN.S194596
19. Ahmadi D, Zarei M, Rahimi M, Khazaie M, Asemi Z, Mir SM, *et al.* Preparation and in-vitro evaluation of pH-responsive cationic cyclodextrin coated magnetic nanoparticles for delivery of methotrexate to the Saos-2 bone cancer cells. *J Drug Deliv Sci Technol* **2020**; 57: 101584. https://doi.org/10.1016/j.jddst.2020.101584
20. Manatunga DC, Godakanda VU, de Silva RM, de Silva KMN. Recent developments in the use of organic–inorganic nanohybrids for drug delivery. *Wiley Interdiscip Rev Nanomed Nanobiotechnol* **2019**; e1605. https://doi.org/10.1002/wnan.1605
21. Guo K, Zhao X, Dai X, Zhao N, Xu FJ. Organic/inorganic nanohybrids as multifunctional gene delivery systems. *J Gene Med* **2019**; 21: e3084. https://doi.org/10.1002/jgm.3084
22. Rahimi M, Shojaei S, Safa KD, Ghasemi Z, Salehi R, Yousefi B, *et al.* Biocompatible magnetic tris(2-aminoethyl)amine functionalized nanocrystalline cellulose as a novel nanocarrier for anticancer drug delivery of methotrexate. *New Journal of Chemistry* **2017**; 41: 2160-8. https://doi.org/10.1039/C6NJ03332F
23. Rahimi M, Charmi G, Matyjaszewski K, Banquy X, Pietrasik J. Recent developments in natural and synthetic polymeric drug delivery systems used for the treatment of osteoarthritis. *Acta Biomater* **2021**; 123: 31-50. https://doi.org/10.1016/j.actbio.2021.01.003
24. Alemi F, Zarezadeh R, Sadigh AR, Hamishehkar H, Rahimi M, Majidinia M, *et al.* Graphene oxide and reduced graphene oxide: Efficient cargo platforms for cancer theranostics. *J Drug Deliv Sci Technol* **2020**; 101974. https://doi.org/10.1016/j.jddst.2020.101974
25. Pan Y, Sahoo NG, Li L. The application of graphene oxide in drug delivery. *Expert Opin Drug Deliv* **2012**; 9: 1365-76. https://doi.org/10.1517/17425247.2012.729575
26. Li J-L, Tang B, Yuan B, Sun L, Wang X-G. A review of optical imaging and therapy using nanosized graphene and graphene oxide. *Biomaterials* **2013**; 34: 9519-34. https://doi.org/10.1016/j.biomaterials.2013.08.066
27. Salatin S, Yari Khosroushahi A. Overviews on the cellular uptake mechanism of polysaccharide colloidal nanoparticles. *J Cell Mol Med* **2017**; 21: 1668-86. https://doi.org/10.1111/jcmm.13110
28. Jiang B. Aerobic glycolysis and high level of lactate in cancer metabolism and microenvironment. *Genes Dis* **2017**; 4: 25-7. https://doi.org/10.1016/j.gendis.2017.02.003
29. Rahimi M, Shafiei-Irannejad V, D. Safa K, Salehi R. Multi-branched ionic liquid-chitosan as a smart and biocompatible nano-vehicle for combination chemotherapy with stealth and targeted properties. *Carbohydr Polym* **2018**; 196: 299-312. https://doi.org/10.1016/j.carbpol.2018.05.059
30. Rahimi M, Ahmadi R, Samadi Kafil H, Shafiei-Irannejad V. A novel bioactive quaternized chitosan and its silver-containing nanocomposites as a potent antimicrobial wound dressing: Structural and biological properties. *Mater Sci Eng C Mater Biol Appl* **2019**; 101: 360-9. https://doi.org/10.1016/j.msec.2019.03.092
31. Guo H-L, Wang X-F, Qian Q-Y, Wang F-B, Xia X-H. A green approach to the synthesis of graphene nanosheets. *ACS Nano* **2009**; 3: 2653-9. https://doi.org/10.1021/nn900227d
32. Jiang X, Lu G, Huang X, Li Y, Cao F, Chen H, *et al.* Thermo-responsive graphene oxide/poly (ethyl ethylene phosphate) nanocomposite via ring opening polymerization. *Nanomaterials (Basel)* **2019**; 9: 207. https://doi.org/10.3390/nano9020207
33. Ahmadian S, Barar J, Saei AA, Fakhree MAA, Omidi Y. Cellular toxicity of nanogenomedicine in MCF-7 cell line: MTT assay. *J Vis Exp* **2009**; e1191. https://doi.org/10.3791/1191
34. Aliyari Z, Soleimanirad S, Sayyah Melli M, Tayefi Nasrabadi H, Nozad Charoudeh H. IL2rg Cytokines Enhance Umbilical Cord Blood CD34+ Cells Differentiation to T Cells. *Adv Pharm Bull* **2015**; 5: 615-9. https://doi.org/10.15171/apb.2015.083
35. Aliyari Z, Alemi F, Brazvan B, Taye fi Nasrabadi H, Charoudeh HN. Cd26+ cord blood mononuclear cells significantly produce B, T, and Nk cells. *Iran J Immunol* **2015**; 12: 16-26.
36. Chaiyakun S, Witit-Anun N, Nuntawong N, Chindaudom P, Oaew S, Kedkeaw C, *et al.* Preparation and characterization of graphene oxide nanosheets. *Procedia Eng* **2012**; 32: 759-64. https://doi.org/10.1016/j.proeng.2012.02.009
37. Dwivedi R, Singh AK, Dhillon A. pH-responsive drug release from dependal-M loaded polyacrylamide hydrogels. *J SCI-ADV MATER DEV* **2017**; 2: 45-50. https://doi.org/10.1016/j.jsamd.2017.02.003
38. Mircioiu C, Voicu V, Anuta V, Tudose A, Celia C, Paolino D, *et al.* Mathematical modeling of release kinetics from supramolecular drug delivery systems. *Pharmaceutics* **2019**; 11: 140. https://doi.org/10.3390/pharmaceutics11030140
39. Loutfy SA, Salaheldin TA, Ramadan MA, Farroh KY, Abdallah ZF, Youssef T. Synthesis, characterization and cytotoxic evaluation of graphene oxide nanosheets: in vitro liver cancer model. *Asian Pac J Cancer Prev* **2017**; 18: 955. https://doi.org/10.22034/APJCP.2017.18.4.955
40. Maleki M, Zarezadeh R, Nouri M, Sadigh AR, Pouremamali F, Asemi Z, *et al.* Graphene Oxide: A Promising Material for Regenerative Medicine and Tissue Engineering. *Biomol Concepts* **2020**; 11: 182-200. https://doi.org/10.1515/bmc-2020-0017
41. Habte AT, Ayele DW. Synthesis and characterization of reduced graphene oxide (rGO) started from graphene oxide (GO) using the tour method with different parameters. *ADV MATER SCI ENG* **2019**; 2019. https://doi.org/10.1155/2019/5058163
42. Pravin M, Gnanamani A. Preparation, characterization and reusability efficacy of amine-functionalized graphene oxide-polyphenol oxidase complex for removal of phenol from aqueous phase. *RSC Adv* **2018**; 8: 38416-24. https://doi.org/10.1039/c8ra06364h
43. Stobinski L, Lesiak B, Malolepszy A, Mazurkiewicz M, Mierzwa B, Zemek J, *et al.* Graphene oxide and reduced graphene oxide studied by the XRD, TEM and electron spectroscopy methods. *J Electron Spectros Relat Phenomena* **2014**; 195: 145-54. https://doi.org/10.1016/j.elspec.2014.07.003
44. Li C, Vongsvivut J, She X, Li Y, She F, Kong L. New insight into non-isothermal crystallization of PVA-graphene composites. *Phys Chem Chem Phys* **2014**; 16: 22145-58. https://doi.org/10.1039/c4cp03613a
45. Deng S, Berry V. Wrinkled, rippled and crumpled graphene: an overview of formation mechanism, electronic properties, and applications. *Mater Today* **2016**; 19: 197-212. https://doi.org/10.1016/j.mattod.2015.10.002
46. Sun L, Fugetsu B. Mass production of graphene oxide from expanded graphite. *Mater Lett* **2013**; 109: 207-10. https://doi.org/10.1016/j.matlet.2013.07.072
47. Zhao X, Jiang X, Peng D, Teng J, Yu J. Behavior and mechanism of graphene oxide-tris (4-aminophenyl) amine composites in adsorption of rare earth elements. J Rare Earths **2021**; 39: 90-7. https://doi.org/10.1016/j.jre.2020.02.006
48. Mousavi SM, Hashemi SA, Ghasemi Y, Amani AM, Babapoor A, Arjmand O. Applications of graphene oxide in case of nanomedicines and nanocarriers for biomolecules: review study. *Drug Metab Rev* **2019**; 51: 12-41. https://doi.org/10.1080/03602532.2018.1522328
49. Kiew SF, Kiew LV, Lee HB, Imae T, Chung LY. Assessing biocompatibility of graphene oxide-based nanocarriers: A review. *J Control Release* **2016**; 226: 217-28. https://doi.org/10.1016/j.jconrel.2016.02.015
50. Vinothini K, Rajendran NK, Munusamy MA, Alarfaj AA, Rajan M. Development of biotin molecule targeted cancer cell drug delivery of doxorubicin loaded κ-carrageenan grafted graphene oxide nanocarrier. *Mater Sci Eng C Mater Biol Appl* **2019**; 100: 676-87. https://doi.org/10.1016/j.msec.2019.03.011
51. Zhao X, Yang L, Li X, Jia X, Liu L, Zeng J, *et al.* Functionalized graphene oxide nanoparticles for cancer cell-specific delivery of antitumor drug. *Bioconjug Chem* **2015**; 26: 128-36. https://doi.org/10.1021/bc5005137
52. Fu Y, Kao WJ. Drug release kinetics and transport mechanisms of non-degradable and degradable polymeric delivery

systems. *Expert Opin Drug Deliv* **2010**; 7: 429-44. https://doi.org/10.1517/17425241003602259

53. Sun X, Liu Z, Welsher K, Robinson JT, Goodwin A, Zaric S, *et al.* Nano-Graphene Oxide for Cellular Imaging and Drug Delivery. *Nano Res* **2008**; 1: 203-12. https://doi.org/10.1007/s12274-008-8021-8
54. Varela-López A, Battino M, Navarro-Hortal MD, Giampieri F, Forbes-Hernández TY, Romero-Márquez JM, *et al.* An update on the mechanisms related to cell death and toxicity of doxorubicin and the protective role of nutrients. *Food Chem Toxicol* **2019**; 134: 110834. https://doi.org/10.1016/j.fct.2019.110834
55. Armstrong J, Dass CR. Doxorubicin Action on Mitochondria: Relevance to Osteosarcoma Therapy? *Curr Drug Targets* **2018**; 19: 432-8. https://doi.org/10.2174/1389450116666150416115852
56. Farhane Z, Bonnier F, Byrne HJ. Monitoring doxorubicin cellular uptake and trafficking using in vitro Raman microspectroscopy: short and long time exposure effects on lung cancer cell lines. *Anal Bioanal Chem* **2017**; 409: 1333-46. https://doi.org/10.1007/s00216-016-0065-0
57. Tacar O, Dass CR. Doxorubicin-induced death in tumour cells and cardiomyocytes: is autophagy the key to improving future clinical outcomes? *J Pharm Pharmacol* **2013**; 65: 1577-89. https://doi.org/10.1111/jphp.12144